

## Accepted Article

**Title:** Dynamics of meso-chiral interconversion in butterfly-shape overcrowded alkene rotor tunable by solvent properties

**Authors:** Masayuki Takeuchi, Atsuro Takai, Jan Labuta, Kalathil K. Kartha, and Zdeněk Futera

This manuscript has been accepted after peer review and appears as an Accepted Article online prior to editing, proofing, and formal publication of the final Version of Record (VoR). This work is currently citable by using the Digital Object Identifier (DOI) given below. The VoR will be published online in Early View as soon as possible and may be different to this Accepted Article as a result of editing. Readers should obtain the VoR from the journal website shown below when it is published to ensure accuracy of information. The authors are responsible for the content of this Accepted Article.

**To be cited as:** *Angew. Chem. Int. Ed.* 10.1002/anie.202102719

**Link to VoR:** <https://doi.org/10.1002/anie.202102719>

## RESEARCH ARTICLE

# Dynamics of meso-chiral interconversion in butterfly-shape overcrowded alkene rotor tunable by solvent properties

Kalathil K. Kartha,<sup>[a]</sup> Atsuro Takai,<sup>[a]</sup> Zdeněk Futera,<sup>[b]</sup> Jan Labuta,<sup>\*[c]</sup> and Masayuki Takeuchi<sup>\*[a]</sup>

[a] Dr. Kalathil K. Kartha, Dr. Atsuro Takai, Prof. Dr. Masayuki Takeuchi  
Molecular Design and Function Group, National Institute for Materials Science (NIMS), 1-2-1 Sengen, Tsukuba, Ibaraki 305-0047, Japan  
E-mail: TAKEUCHI.Masayuki@nims.go.jp

[b] Dr. Zdeněk Futera  
University of South Bohemia, Faculty of Science, Branišovská 1760, 370 05 České Budějovice, Czech Republic

[c] Dr. Jan Labuta  
World Premier International Center for Materials Nanoarchitectonics (WPI-MANA), National Institute for Materials Science (NIMS), 1-1 Namiki, Tsukuba, Ibaraki 305-0044, Japan  
E-mail: LABUTA.Jan@nims.go.jp

Supporting information for this article is given via a link at the end of the document.

**Abstract:** Control over dynamic motion at the molecular level and stimuli-responsiveness are important issues for making nano-motors, nano-actuators or nano-sensors. Elucidation of dynamics of molecular rotational motion is an essential part and still challenging area of research. In this report, demonstration of reversible diastereomeric interconversion of a molecular rotor composed of overcrowded butterfly-shape alkene (**FDf**) is given. Its inherent dual rotatory motion (two rotors, one stator) with interconversion between two diastereomers, chiral *trans*-**FDf** and meso *cis*-**FDf** forms, has been examined in detail upon varying temperatures and solvents. The free energy profile of 180° revolution of one rotor part has a bimodal shape with unevenly positioned maxima (i.e. transition states). **FDf** in aromatic solvents adopts preferentially meso *cis*-conformation, while in non-aromatic solvents a chiral *trans*-conformation is more abundant due to the solvent interactions with peripheral hexyl chains (solvophobic effect). Additionally, moderate correlations between the *trans*-**FDf**/*cis*-**FDf** ratio and solvent parameters, such as refractive index, polarizability, and viscosity were found. The results presented here have implementations in several fields of organic chemistry, such as the design of artificial molecular machines, asymmetric/stereoselective reactions and solvent properties scales.

## Introduction

Nature is abundant with molecular rotors, such as ATP synthases<sup>1,2</sup> and other intracellular motors,<sup>2,3</sup> that inspire chemists to design various artificial molecular machines,<sup>4-7</sup> such as molecular motors,<sup>8,9</sup> rotors,<sup>10</sup> ratchets,<sup>11</sup> gears,<sup>12,13</sup> breaks,<sup>14</sup> shuttles,<sup>15</sup> stirrers,<sup>16</sup> turnstiles,<sup>17</sup> torsion balances,<sup>18,19</sup> viscosity probes,<sup>20</sup> or molecular machine based artificial muscles.<sup>21</sup> Elucidation of molecular rotational motion is still a challenging area of research, especially when multimodal rotation (two or more rotating parts) occurs simultaneously.<sup>8</sup> Moreover, achieving the correct or intended performance of molecular systems by solvent properties, such as viscosity and polarity, is also an important issue. There are numerous cases reporting strong solvent effects, such as a 200-fold increased rate of shuttling in the peptide rotaxane system upon adding a small amount of methanol into the dichloromethane solution,<sup>15</sup> and solvent viscosity dependent speed of rotation of overcrowded alkene

molecular stirrer.<sup>16</sup> There are also profound solvent effects on *cis-trans* or *Z-E* isomerization switching processes,<sup>22</sup> for example thermally stable *E*-isomer of dipyrinone in methanol compared to thermally reversible *Z-E* transition of dipyrinone in chloroform,<sup>23</sup> or solvent effects on *Z-E* equilibrium of azobenzenes.<sup>24</sup> Despite these recent advances in solvent-responsive molecular systems, however, limited molecular design of multimodal rotors hinder the elucidation of their dynamical processes and the correlations of the dynamical behaviour with solvent parameters. In this context, we focused on the concept of overcrowded alkenes for construction of a dual rotatory system. We envisioned that introducing a planar  $\pi$ -system (a stator unit) in between two rotor units would induce multimodal diastereomeric interconversion processes that can be monitored using NMR spectroscopy. Such a molecular rotor is expected to be a dynamic molecular probe in which several isomers are precisely distinguishable, thermodynamically stable, and tunable by external stimuli, such as temperature, additive, and solvent type.

Herein we report an overcrowded aromatic hydrocarbon rotor, **FDf** (Figure 1a), wherein two fluorenylidene (FLU: rotor units) are connected with dihydro-indenoidene (DHI: a stator unit)<sup>25,26</sup> through a rotatable C=C double bond.<sup>27,28</sup> Two distinct flipping motions of **FDf** and their kinetics in solution were investigated by means of variable temperature (VT) NMR spectroscopy, DFT calculations and classical molecular dynamics simulations. Furthermore, we have found that the ratio of the two interconverting diastereomeric forms of **FDf**, the chiral *trans*-**FDf** form and meso *cis*-**FDf** form, is strongly associated with the type of solvent or composition of the binary solvent mixture used. Presented results reveal the mechanism of diastereomeric interconversion processes in the **FDf** molecule and the effects which influence these.

## Results and Discussion

The synthesis<sup>29,30</sup> and characterization of **FDf** were summarised in Supporting Information (Figures S1–S13). **FDf** exists in *cis* and *trans* conformations (diastereomers) (Figure 1a,b) where the angle between DHI and FLU units is about 35° as obtained from DFT optimized structures (see Quantum mechanical calculations

## RESEARCH ARTICLE

in Supporting Information). The *cis*-isomer has one meso form (*P,M*)-**FDF**, identical to (*M,P*)-**FDF**. The *trans*-isomer has two chiral forms: (*P,P*)-**FDF** and (*M,M*)-**FDF**. There is a temperature and solvent type dependent interconversion of these forms, as discussed below. The assignment of NMR spectra to corresponding *cis/trans* diastereomers has been done using 2D NMR measurements (Figures S14–S17) and DFT calculated chemical shifts (Table S2 and Figures S22–S30).<sup>31,32</sup>

Variable temperature (VT) NMR measurements performed in high boiling point solvents, such as *o*-dichlorobenzene-*d*<sub>4</sub> (ODCB) (Figure 1c,d) and toluene-*d*<sub>8</sub> (Figure S18) showed sharp split resonances at 25 °C. The **FDF** molecules in ODCB are present in two (*cis* and *trans*) diastereomeric forms in an equimolar ratio, as seen in NMR spectrum at 25 °C (Figure 1c), i.e. the resonances corresponding to *trans*- and *cis*-form (e.g. A<sup>t</sup>, A<sup>c</sup> or E<sup>t</sup>, E<sup>c</sup>) have the same area. This implies that (*P,M*)-**FDF** (2×), (*P,P*)-**FDF** (1×), and (*M,M*)-**FDF** (1×) have a statistical distribution in ODCB. Two distinct coalescences at different temperature

scales were observed upon heating, as shown in Figure 1c (lower temperature: from 25 °C to ca. 100 °C) and Figure 1d (higher temperature: ca. 75 °C to 150 °C). The low-temperature line-shape changes of DHI and FLU resonances (e.g. A<sup>t</sup>, A<sup>c</sup>, E<sup>t</sup>, and E<sup>c</sup>) correspond to a diastereomeric interchange between the chiral *trans*-**FDF** and meso *cis*-**FDF** forms via the flip of FLU unit over the rim of DHI unit, hereafter named as the "rim flip" mechanism (Figure 1a). The transition state TS<sub>r</sub><sup>‡</sup> adopts a geometry in which DHI and one FLU unit are coplanar. The high-temperature coalescence (e.g. FLU resonances E and F in Figure 1d) is associated with the rotation of a FLU unit around the double bond through transition state TS<sub>d</sub><sup>‡</sup> in which DHI and FLU units are perpendicular to each other, hereafter named as the "double bond flip" mechanism (Figure 1b). When the double bond flip process starts to be detectable, the *trans* and *cis* diastereomeric forms are already indistinguishable in the NMR spectrum due to fast exchange regime (i.e. resonances A<sup>t</sup>, A<sup>c</sup> → A, and E<sup>t</sup>, E<sup>c</sup> → E, etc.).

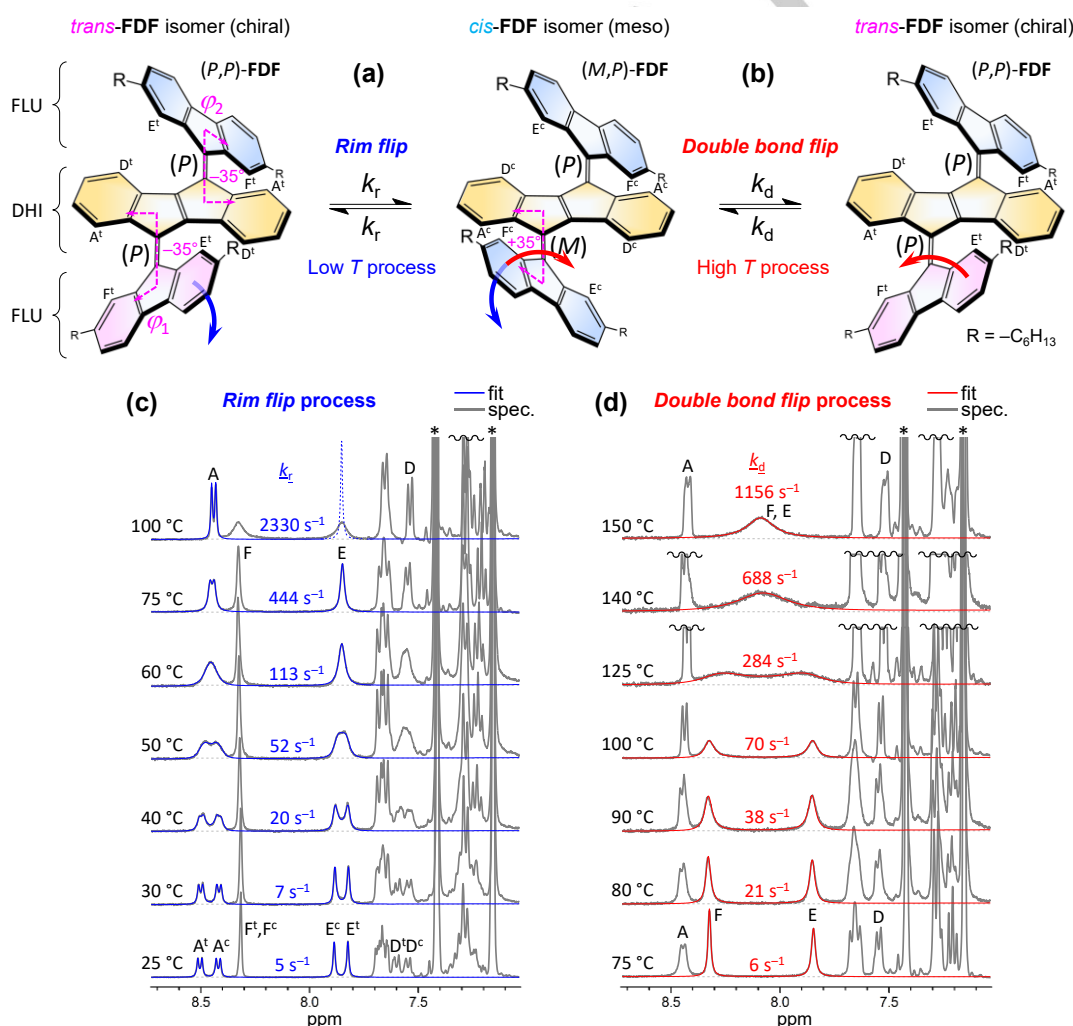


**Figure 1.** Structure of butterfly-shape **FDF** with the description of flipping processes, including their NMR spectral manifestations. a, b) Stereochemical structures of **FDF** isomers during *cis-trans* interconversion via (a) rim flip and (b) double bond flip mechanism. Oriented values of torsion angles  $\phi_1$  and  $\phi_2$  as obtained from DFT are shown in (a). c) VT <sup>1</sup>H NMR spectra (400 MHz, grey line) of the aromatic part of **FDF** (7 mM, ODCB) showing the low temperature rim flip process. Line-shapes of A<sup>t</sup>, A<sup>c</sup> and E<sup>t</sup>, E<sup>c</sup> resonances, respectively, are fitted using a two-site symmetrical exchange (blue line). Note that at 100 °C, the E resonance is broadened due to the onset of the double bond flip process (drawn dashed blue line represents only rim flip process consistent with the fitting of A<sup>t</sup> and A<sup>c</sup> resonances). Therefore, the  $k_r$  value was determined only from fits of A<sup>t</sup> and A<sup>c</sup> resonances which are not affected by the double bond flip process. d) VT <sup>1</sup>H NMR spectra (400 MHz, grey line) of the aromatic part of **FDF** (7 mM, ODCB) showing the high temperature double bond flip process. Line-shapes of F and E resonances are fitted using a two-site symmetrical exchange (red line). Notes: Superscripts 'c' and 't' denote *cis*- and *trans*-isomers. Intensity scales (y-axes) are uneven to emphasize spectral features around coalescence temperature. Values of rate constants  $k_r$  and  $k_d$  are given at each spectrum. For resonance assignment, see structures at the top. For a more comprehensive assignment of <sup>1</sup>H NMR spectrum, see Figure S14.

## RESEARCH ARTICLE

In order to determine exchange rates and energy barriers of these two processes, we focused on the analysis of VT NMR spectral line-shapes and employed a two-site symmetrical exchange model (due to *cis/trans* equimolar ratio in ODCB). Hereafter, the 'r' and 'd' subscripts denote the rim flip and double bond flip processes, respectively. Each process has a characteristic temperature-dependent value of mean exchange rate  $k_r$  and  $k_d$  (in  $s^{-1}$ ) (Figures 1a,b). We used the symmetric exchange spectral pattern of two singlets<sup>33-35</sup> as described together with the fitting procedure in details in Supporting Information. The line-shape fitting is shown in Figures 1c,d (blue and red lines) and obtained rate constants are plotted in Figure S19.

The kinetics of the unimolecular interconversion process is described by Eyring equation.<sup>36</sup>

$$k = \frac{k_B T}{h} e^{-\frac{\Delta G^\ddagger}{RT}} = \frac{k_B T}{h} e^{-\frac{\Delta H^\ddagger}{RT}} e^{\frac{\Delta S^\ddagger}{R}} \quad (1)$$

Where  $k$  (represents  $k_r$  or  $k_d$ ) is the exchange rate constants of reversible symmetric reaction,  $k_B$  is the Boltzmann constant,  $h$  is the Planck constant,  $R$  is the gas constant, and  $T$  is the absolute temperature.  $\Delta G^\ddagger = \Delta H^\ddagger - T\Delta S^\ddagger$  (represents  $\Delta G_r^\ddagger$  or  $\Delta G_d^\ddagger$ ) are the Gibbs free energy of activation to reach the transition state ( $TS_r^\ddagger$  or  $TS_d^\ddagger$ ). The  $\Delta H^\ddagger$  and  $\Delta S^\ddagger$  are the enthalpy and entropy of activation, respectively, for the corresponding flipping process. The kinetic parameters as obtained from an Eyring plot (i.e. plot of  $\ln(k/T)$  vs.  $1/T$ ) are shown in Figure 2 and Table S1.

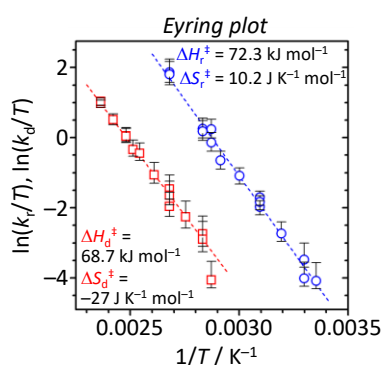


**Figure 2.** Eyring plots of exchange rates  $k_r$  (blue circles) and  $k_d$  (red squares) with values of activation enthalpies and entropies indicated. Room temperature barrier heights for rim flip and double bond flip process are  $\Delta G_r^\ddagger(25^\circ\text{C}) = 69.2$  kJ mol<sup>-1</sup> and  $\Delta G_d^\ddagger(25^\circ\text{C}) = 76.8$  kJ mol<sup>-1</sup>, respectively.

The linearity of the Eyring plots of both processes indicates that they involve only one simple mechanism with one transition state. Therefore, the rim flip and double bond flip are independent processes. It is quite remarkable that, at first glance, the complex dynamics can be effectively 'deconvoluted' using NMR line-shape analyses. There are several positive coincidences: (i) the NMR resonances corresponding to each process do not overlap; (ii) there are some resonances that can be unambiguously attributed to just one process; and (iii) the rates of the dynamical processes are within the range of an NMR chemical shift time scale (i.e. having barriers of transition  $\Delta G^\ddagger(25^\circ\text{C})$  around 65 kJ mol<sup>-1</sup>).<sup>13,37,38</sup>

The experimental activation energy of rim flip and double bond flip process (at 25°C) is  $\Delta G_r^\ddagger(25^\circ\text{C}) = 69.2$  kJ mol<sup>-1</sup> and  $\Delta G_d^\ddagger(25^\circ\text{C}) = 76.8$  kJ mol<sup>-1</sup>, respectively. The activation energies as

obtained from DFT calculated total energy profile (Figure 3) are  $\Delta E_r^\ddagger(0\text{ K})^{\text{DFT}} = 78.7$  kJ mol<sup>-1</sup> and  $\Delta E_d^\ddagger(0\text{ K})^{\text{DFT}} = 86.3$  kJ mol<sup>-1</sup>. The DFT Gibbs free-energy corrections ( $\Delta G$ ) were also calculated at 25 °C at stationary points using vibrational modes yielding  $\Delta G_r^\ddagger(25^\circ\text{C})^{\text{DFT}} = 83.3$  kJ mol<sup>-1</sup> and  $\Delta G_d^\ddagger(25^\circ\text{C})^{\text{DFT}} = 86.7$  kJ mol<sup>-1</sup>. The experimental and calculated values are in acceptable agreement, as shown in Figure 3 (and summarized in Table S1). It should be noted that the total energy profile ( $\Delta E$ ) in Figure 3 is a good approximation to the Gibbs free energy since the corrections to  $\Delta G$  calculated based on vibrational modes might introduce extra errors, especially for molecules where soft vibrational modes are present due to the internal motions.<sup>38</sup>

The two-dimensional Gibbs free energy surface can be seen in Figure S20. The energetic dependence on both reaction coordinates (angles  $\varphi_1$  and  $\varphi_2$  associated with a rotation of each FLU unit) show broad minima and also suggests that energetic pathways for the *cis-trans* interconversion are statistically favoured over direct *cis-cis* or *trans-trans* interconversion, involving simultaneous rotation of both FLU units.

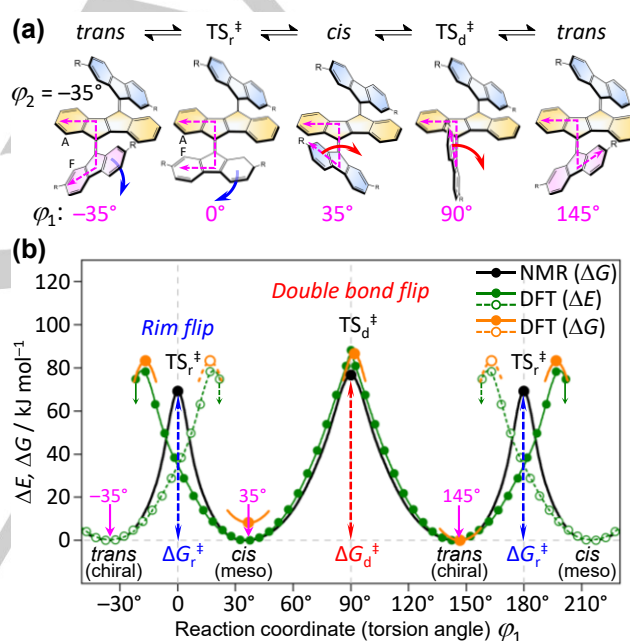


**Figure 3.** Schematic structural changes and energy barrier diagram of FDF during the flipping processes as obtained from NMR and DFT. a) Structural changes of FDF during *trans*→*cis*→*trans* interconversion via rim flip and double bond flip mechanism. b) Gibbs free energy ( $\Delta G$ ) at 25 °C as obtained from NMR (solid black circles). NMR free energy profile along the  $\varphi_1$  reaction coordinate (black line) is shape-wise derived from the DFT calculated profile. DFT total energy profile ( $\Delta E$ ) as calculated at  $\omega\text{B97XD}/6\text{-}311\text{G(d)}/6\text{-}311++\text{G(d,p)}$  level with  $\varphi_2 = -35^\circ$  and constrained torsion angle  $\varphi_1$  (solid green circles and line denote actual calculated values; empty green circles and dashed lines denote values which are symmetrically extended). The 'sawtooth' jumps around  $\varphi_1 = 0^\circ$  and  $180^\circ$  are due to strong steric hindrance of the A and F hydrogen atoms during the DFT constrained calculations. DFT Gibbs free energy ( $\Delta G$ ) corrections were calculated at stationary points at  $\omega\text{B97XD}/6\text{-}311\text{G(d)}$  level based on of gas-phase vibrational modes. A simplified FDF structure ( $\text{C}_6\text{H}_{13}$  alkyl chains were replaced with methyl groups) was used in the DFT calculations.

The activation entropy in the interconversion processes where no bond breaking occurs is expected to have a near-zero value.<sup>38</sup> Considering the experimental error, the rim flip process with activation entropy  $\Delta S_r^\ddagger = 10.2 \pm 7.0$  J mol<sup>-1</sup> K<sup>-1</sup> meets the expectation. On the other hand, the double bond flip process is accompanied by an appreciable negative activation entropy  $\Delta S_d^\ddagger$

## RESEARCH ARTICLE

=  $-27.0 \pm 4.9 \text{ J mol}^{-1} \text{ K}^{-1}$ , indicating that there is increasing order during the formation of  $\text{TS}_d^\ddagger$  transition state. This behaviour suggests that the alkyl  $\text{C}_6\text{H}_{13}$  chains at the periphery of **FDf** play an important role during the double bond flip, where they adopt a particular arrangement to allow for the transition state formation. A lack of alkyl chains in similar bifluorenylidene molecule shows a near-zero activation entropy ( $\Delta S^\ddagger \sim 2.5 \text{ J mol}^{-1} \text{ K}^{-1}$ ) during a similar double bond flip,<sup>28</sup> confirming an adverse effect of alkyl chains for the formation of transition state and effectively slowing down the double bond flip process. To further support the alkyl chains' adverse entropic effect, molecular dynamics (MD) simulations<sup>39</sup> were performed on **FDf** in ODCB at 25 °C. Obtained distributions of end-to-end distances of alkyl chains located at the opposite FLU units in the  $\text{TS}_d^\ddagger$  indicate increased steric hindrance (compared to *cis* or *trans* state) as seen in Figure S41. This effect is not observed for the rim flip process (Figure S41c,d), indicating that the conformational space of alkyl chains is restricted in the  $\text{TS}_d^\ddagger$ , which is the source of reduced entropy.

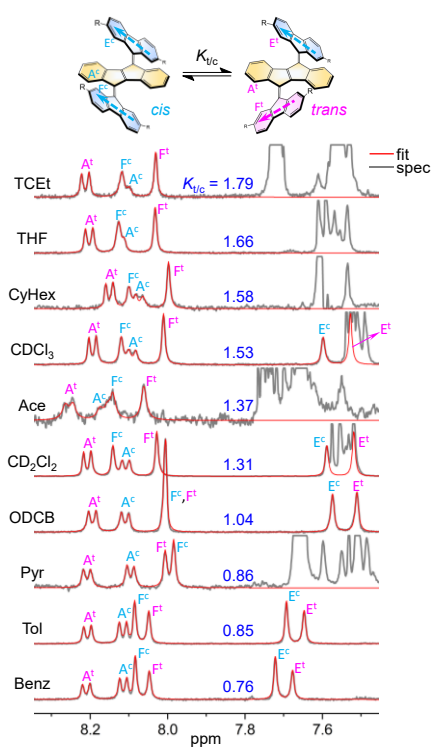


**Figure 4.**  $^1\text{H}$  NMR spectra (400 MHz, 25 °C, grey line: spectrum, red line: fit) of aromatic part of **FDf** (7 mM) in various solvents with values of  $K_{t/c}$  indicated at each spectrum. Legend: TCEt = 1,1,2,2-tetrachloroethane- $d_2$ , THF = tetrahydrofuran- $d_6$ , CyHex = cyclohexane- $d_{12}$ ,  $\text{CDCl}_3$  = chloroform- $d_1$ , Ace = acetone- $d_6$  (low solubility),  $\text{CD}_2\text{Cl}_2$  = dichloromethane- $d_2$ , ODCB = *o*-dichlorobenzene- $d_4$ , Pyr = pyridine- $d_5$ , Tol = toluene- $d_6$ , Benz = benzene- $d_6$ . For clarity the spectra in aromatic solvents were offset upfield (max. 0.27 ppm for pyridine).

Interestingly, when different solvents are used, the ratio between *trans*- and *cis*-form deviates from unity (equimolarity) as seen in  $^1\text{H}$  NMR spectra at 25 °C (Figure 4). The spectra clearly show that in 1,1,2,2-tetrachloroethane- $d_2$  (TCEt) the *trans*-form is more abundant than the *cis*-form (see, for example, resonances,  $\text{F}^1$ ,  $\text{F}^0$  or  $\text{A}^1$ ,  $\text{A}^0$ ). Contrarily, the strongest preference for the *cis*-form can be seen in benzene- $d_6$ . This behaviour was quantitatively examined in different solvents using line-shape

fitting and integrating the area under A and F (and where possible E) resonances in NMR spectra, as seen in Figure 4. This analysis yields the diastereomeric ratio  $K_{t/c}$  of the *trans*-form as compared to the *cis*-form, which is defined as

$$K_{t/c} = \frac{f_t}{f_c} = e^{-\frac{\Delta G_{t/c}}{RT}} \quad (2)$$

and can also be interpreted as an equilibrium constant of the *cis*-*trans* interconversion reaction (Figure 4, top).  $f_t$  and  $f_c$  values are molar fractions of the *trans*- and *cis*-form, respectively, as obtained from NMR integration. The  $\Delta G_{t/c}$  is the Gibbs free energy change of the *cis*-*trans* interconversion reaction, describing the energy difference between *trans*- and *cis*-isomer (for example,  $\Delta G_{t/c}$  is negative when *trans*-form is energetically lower than *cis*-form and vice versa; for more details, see Figure S35).

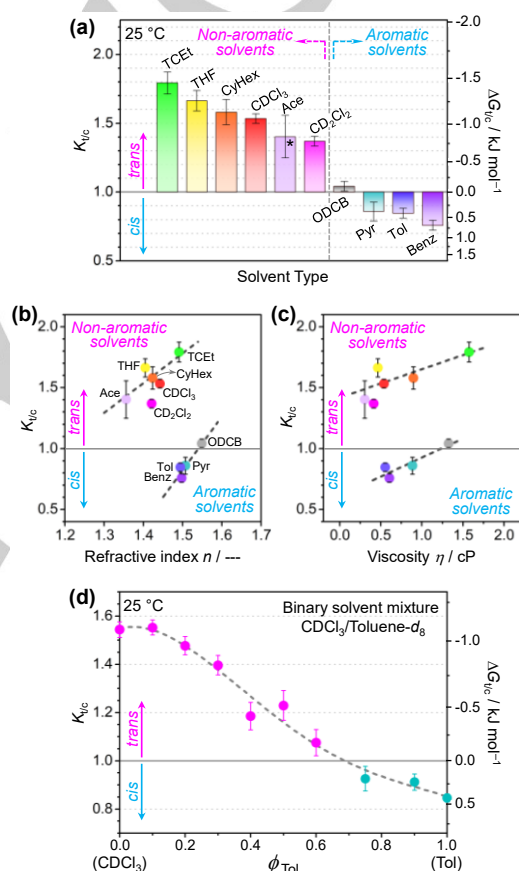


**Figure 5.** Solvent effects on the **FDf** isomerization process. a) Plot of  $K_{t/c}$  and  $\Delta G_{t/c}$  values in various solvents at 25 °C as obtained from fitting of spectra (red curves) in Figure 4. Error bars (st. dev.) are connected with the left axis. Actual values and standard deviations are listed in Table S5. The legend for abbreviations is the same as in Figure 4. The asterisk denotes low solubility of **FDf** in acetone- $d_6$ . b) Correlation between  $K_{t/c}$  and refractive index  $n$ . c) Correlation between  $K_{t/c}$  and viscosity  $\eta$ . (The legend is the same as in Figure 4.) d) Plot of  $K_{t/c}$  and  $\Delta G_{t/c}$  for continuous variation of volume fraction  $\phi_{\text{Tol}}$  of toluene- $d_6$  in  $\text{CDCl}_3$  at 25 °C (for actual NMR spectra see Figure S34).

The  $K_{t/c}$  and  $\Delta G_{t/c}$  values are plotted in Figure 5a (for actual values, see Table S5) and show large solvent dependent variations in the diastereomeric composition of **FDf**. Interestingly, **FDf** prefers the *trans* conformation in non-aromatic solvents and *cis* in aromatic solvents. The correlations between the diastereomeric ratio  $K_{t/c}$  and solvent parameters, such as donor

## RESEARCH ARTICLE

number, acceptor number, dielectric constant, dipole moment, refractive index, polarizability, viscosity, specific heat capacity, relative polarity,  $E_T(30)$  polarity scale, molecular weight, density or Hildebrand and Hansen solubility parameters were investigated. However, no significant correlation across all solvents was found. The correlations for non-aromatic and aromatic solvents, when analyzed separately, show three moderate correlations between  $K_{vic}$  and the solvents' refractive index, viscosity (Figure 5b,c) or polarizability (see Figure S32b).

To explain the mechanism of solvent-induced *cis/trans* interconversion, we have performed MD simulations on **FDf** molecule in all studied solvents at 25 °C (for details, see Section 10 in Supporting information). It turned out that the alkyl side chains play a critical role in the observed behaviour. Aromatic non-polar solvents keep the alkyl chains solvated and in extended form, making the *cis*-form enthalpically favoured. Contrarily, polar non-aromatic solvents show repulsive interactions towards alkyl chains, which tend to shrink and sterically interact between themselves. It induces entropic force towards conformation change to the state with higher entropy (i.e. *trans*-form with higher surface area and alkyl chains more apart. Overall, the solvent-induced interconversion is attributed mainly to the solvophobic interactions between solvent molecules and peripheral alkyl chains. Moreover, the MD simulated tendencies are in good agreement with experimentally observed data (compare Figure 5a and Fig. S39).

Finally, we studied the  $^1\text{H}$  NMR spectra upon changing the volume fraction of toluene- $d_8$  in  $\text{CDCl}_3$  ( $\phi_{\text{tol}}$ ), because two solvents (toluene- $d_8$  and  $\text{CDCl}_3$ ) exhibit a strong preference of **FDf** for *cis*- or *trans*-isomer, respectively (Figure S34). The plot of the extracted  $K_{vic}$  values has nonlinear but continuous dependence of  $K_{vic}$  on the fraction  $\phi_{\text{tol}}$  (Figure 5d). This also shows that the *cis-trans* conformational equilibrium of **FDf** can also be finely tuned to the required *cis/trans* ratio  $K_{vic}$  (in contrast to jump-like changes in different solvents).

## Conclusion

In conclusion, we have shown that **FDf** aromatic hydrocarbon possesses nontrivial bimodal dynamical behaviour involving rim flip and double bond flip processes. Both are connected with diastereomeric interconversion between the chiral *trans*-**FDf** and meso *cis*-**FDf** forms. We were able to separate and analyze the rates of these two processes in a broad range of temperatures using line-shape analysis of  $^1\text{H}$  NMR spectra. Moreover, together with the DFT calculations, a comprehensive kinetic description of **FDf** conformational behaviour was presented. It was shown that **FDf** in various solvents has uneven populations of *cis*- and *trans*-form in a slow exchanging mode (on the NMR time scale) at room temperature. Moreover, **FDf** in aromatic solvents preferentially adopts a meso *cis*-form, whereas in non-aromatic solvents a chiral *trans*-form is preferred. This effect was attributed to solvophobic interactions between solvent molecules and peripheral hexyl chains, as revealed by MD simulations. Additionally, moderate correlations between solvent parameters, such as refractive index, polarizability, and viscosity, and the *trans*-**FDf**/*cis*-**FDf** ratio were shown. The findings presented here have connections in various fields of organic chemistry, such as the design of artificial molecular machines based on sterically

crowded alkenes, solvent properties scales, enantioenrichment reactions, asymmetric or stereoselective reactions, for example, in a search for suitable functionalization conditions (e.g. solvent type, temperature) for chiral-meso interconvertible molecules in order to obtain targeted stereochemical structure of a product.

## Acknowledgements

We are grateful to Dr. Takeshi Yasuda (NIMS), Dr. Takashi Kajitani (Tokyo Tech.), and Prof. Takanori Fukushima (Tokyo Tech.) for their efforts on the physicochemical studies of **FDf** in the solid states. Dr. Manas Bera (NIMS) is greatly acknowledged for his contribution in the initial stages of this work. This research was supported by KAKENHI Grant-in-Aid for Scientific Research (No. 19K05229 for J.L.); Innovative Areas "π-System Figuration" Grant (No. 26102009 and No. 15K21721 for M.T.) from JSPS; Grant-in-Aid for Transformative Research Areas (A) "Condensed Conjugation" from MEXT (20H05868 for M.T.); and the MEXT "NIMS Molecule and Material Synthesis Platform" program.

## Conflict of interest

The authors declare no conflict of interest.

**Keywords:** conformation analysis • crowded alkene • chirality • diastereomers • solvent effects

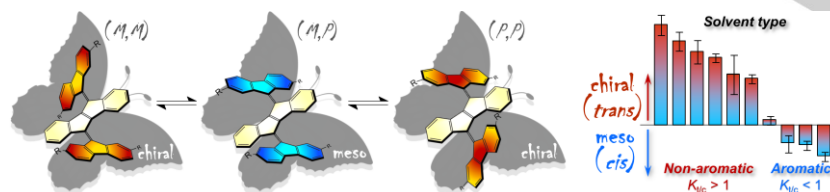
- [1] P. D. Boyer, *Nature* **1999**, *402*, 247-249.
- [2] K. Kinbara, T. Aida, *Chem. Rev.* **2005**, *105*, 1377-1400.
- [3] R. D. Vale, R. A. Milligan, *Science* **2000**, *288*, 88-95.
- [4] M. A. Watson, S. L. Cockroft, *Chem. Soc. Rev.* **2016**, *45*, 6118-6129.
- [5] R. Merindol, A. Walther, *Chem. Soc. Rev.* **2017**, *46*, 5588-5619.
- [6] G. S. Kottas, L. I. Clarke, D. Horinek, J. Michl, *Chem. Rev.* **2005**, *105*, 1281-1376.
- [7] D. Dattler, G. Fuks, J. Heiser, E. Moulin, A. Perrot, X. Yao, N. Giuseppone, *Chem. Rev.* **2020**, *120*, 310-433.
- [8] J. C. M. Kistemaker, P. Štacko, J. Visser, B. L. Feringa, *Nat. Chem.* **2015**, *7*, 890-896.
- [9] N. Koumura, R. W. J. Zijlstra, R. A. van Delden, N. Harada, B. L. Feringa, *Nature* **1999**, *401*, 152-155.
- [10] A. M. Schoevaars, W. Kruizinga, R. W. J. Zijlstra, N. Veldman, A. L. Spek, B. L. Feringa, *J. Org. Chem.* **1997**, *62*, 4943-4948.
- [11] T. R. Kelly, I. Tellitu, J. P. Sestelo, *Angew. Chem. Int. Ed. Engl.* **1997**, *36*, 1866-1868.
- [12] H. Ube, Y. Yasuda, H. Sato, M. Shionoya, *Nat. Commun.* **2017**, *8*, 14296.
- [13] S. Grilli, L. Lunazzi, A. Mazzanti, G. Mazzanti *J. Org. Chem.* **2001**, *66*, 748-754.
- [14] T. Tseng, H.-F. Lu, C.-Y. Kao, C.-W. Chiu, I. Chao, C. Prabhakar, J.-S. Yang, *J. Org. Chem.* **2017**, *82*, 5354-5366.
- [15] A. S. Lane, D. A. Leigh, A. Murphy, *J. Am. Chem. Soc.* **1997**, *119*, 11092-11093.
- [16] J. Chen, J. C. M. Kistemaker, J. Robertus, B. L. Feringa, *J. Am. Chem. Soc.* **2014**, *136*, 42, 14924-14932.
- [17] T. C. Bedard, J. S. Moore, *J. Am. Chem. Soc.* **1995**, *117*, 10662-10671.
- [18] E. Kim, S. Paliwal, C. S. Wilcox, *J. Am. Chem. Soc.* **1998**, *120*, 11192-11193.
- [19] S. L. Cockroft, C. A. Hunter, *Chem. Commun.* **2006**, 3806-3808.
- [20] W. L. Goh, M. Y. Lee, T. L. Joseph, S. T. Quah, C. J. Brown, C. Verma, S. Brenner, F. J. Ghadessy, Y. N. Teo, *J. Am. Chem. Soc.* **2014**, *136*, 6159-6162.
- [21] G. Du, E. Moulin, N. Jouault, E. Buhler, N. Giuseppone, *Angew. Chem., Int. Ed.* **2012**, *51*, 12504-12508.

## RESEARCH ARTICLE

- [22] C. Dugave, L. Demange, *Chem. Rev.* **2003**, *103*, 2475-2532.
- [23] Y. Sakata, S. Fukushima, S. Akine, J. Setsune, *Chem. Commun.*, **2016**, 52, 1278-1281.
- [24] H. M. D. Bandara, S. C. Burdette, *Chem. Soc. Rev.* **2012**, *41*, 1809-1825.
- [25] T. Kawase, T. Kawase, T. Fujiwara, C. Kitamura, A. Konishi, Y. Hirao, K. Matsumoto, H. Kurata, T. Kubo, S. Shinamura, H. Mori, E. Miyazaki, K. Takimiya, *Angew. Chem., Int. Ed.* **2010**, *49*, 7728-7732.
- [26] T. Kawase, J. Nishida, *Chem. Rec.* **2015**, *15*, 1045-1059.
- [27] J. Xu, A. Takai, A. Bannaron, T. Nakagawa, Y. Matsuo, M. Sugimoto, Y. Matsushita, M. Takeuchi, *Mater. Chem. Front.* **2018**, *2*, 780-784.
- [28] We have reported that a 9,9'-bifluorenylidene derivative, one of the simplest overcrowded alkenes, exhibits thermal isomerization by rotation around the central C=C double bond which we assessed quantitatively by VT NMR measurements: A. Takai, D. J. Freas, T. Suzuki, M. Sugimoto, J. Labuta, R. Haruki, R. Kumai, S. Adachi, H. Sakai, T. Hasobe, Y. Matsushita, M. Takeuchi, *Org. Chem. Front.* **2017**, *4*, 650-657.
- [29] S. Song, Y. Jin, S. H. Kim, J. Moon, K. Kim, J. Y. Kim, S. H. Park, K. Lee, H. Suh, *Macromolecules*, **2008**, *41*, 7296-7305.
- [30] M. Nakano, I. Osaka, K. Takimiya, T. Koganezawa, *J. Mater. Chem. C* **2014**, *2*, 64-70.
- [31] J.-D. Chai, M. Head-Gordon, *Phys. Chem. Chem. Phys.* **2008**, *10*, 6615-6620.
- [32] Frisch, M. J. et al. Gaussian 09, Revision A.1 (Gaussian, Inc., Wallingford, CT, 2010).
- [33] H. S. Gutowsky, A. Saika, *J. Chem. Phys.* **1953**, *21*, 1688-1694.
- [34] J. Labuta, Z. Futera, S. Ishihara, H. Kouřilová, Y. Tateyama, K. Ariga, J. P. Hill, *J. Am. Chem. Soc.* **2014**, *136*, 2112-2118.
- [35] V. Římal, H. Štěpánková, J. Štěpánek, *Concepts Magn. Reson. Part A*, **2011**, *38*, 117-127.
- [36] S. Glasstone, K. J. Laidler, H. Eyring, *The Theory of Rate Processes*, pp. 199 (McGraw-Hill Book Company, New York and London, 1941).
- [37] I. K. Mati, S. L. Cockroft, *Chem. Soc. Rev.* **2010**, *39*, 4195-4205.
- [38] D. Casarini, L. Lunazzi, A. Mazzanti, *Eur. J. Org. Chem.* **2010**, 2035-2056.
- [39] D. A. Case et al.: Amber 2016 (University of California, San Francisco, 2016).

## RESEARCH ARTICLE

## Entry for the Table of Contents



**Butterfly-shape overcrowded alkene rotor** was synthesized, and its meso-chiral diastereomeric interconversion processes were elucidated in different solvents. The interconversion has nontrivial bimodal dynamics involving two mechanisms, "rim flip" and "double bond flip". The rotor shows a preference for meso *cis*-conformation in aromatic solvents and chiral *trans*-conformation in non-aromatic solvents.